2-2012

Time-Dependent Fatigue Crack Propagation Behavior of Two Solid-Solution-Strengthened Ni-Based Superalloys—INCONEL 617 and HAYNES 230

Longzhou Ma
University of Nevada, Las Vegas, lma@unlv.nevada.edu

Shawoon K. Roy
University of Nevada, Las Vegas

Muhammad H. Hasan
Taibah University

Joydeep Pal
General Electric

Sudin Chatterjee
Tata Steel Ltd

Time-Dependent Fatigue Crack Propagation Behavior of Two Solid-Solution-Strengthened Ni-Based Superalloys—INCONEL 617 and HAYNES 230

LONGZHOU MA, SHAWOON K. ROY, MUHAMMAD H. HASAN, JOYDEEP PAL, and SUDIN CHATTERJEE

The fatigue crack propagation (FCP) as well as the sustained loading crack growth (SLCG) behavior of two solid-solution-strengthened Ni-based superalloys, INCONEL 617 (Special Metals Corporation Family of Companies) and HAYNES 230 (Haynes International, Inc., Kokomo, IN), were studied at increased temperatures in laboratory air under a constant stress-intensity-factor (K) condition. The crack propagation tests were conducted using a baseline cyclic triangular waveform with a frequency of $\frac{1}{3}$ Hz. Various hold times were imposed at the maximum load of a fatigue cycle to study the hold time effect. The results show that a linear elastic fracture mechanics (LEFM) parameter, stress intensity factor (K), is sufficient to describe the FCP and SLCG behavior at the testing temperatures ranging from 873 K to 1073 K (600 °C to 800 °C). As observed in the precipitation-strengthened superalloys, both INCONEL 617 and HAYNES 230 exhibited the time-dependent FCP, steady SLCG behavior, and existence of a damage zone ahead of crack tip. A thermodynamic equation was adapted to correlate the SLCG rates to determine thermal activation energy. The fracture modes associated with crack propagation behavior were discussed, and the mechanism of time-dependent FCP as well as SLCG was identified. Compared with INCONEL 617, the lower crack propagation rates of HAYNES 230 under the time-dependent condition were ascribed to the different fracture mode and the presence of numerous W-rich M_6C-type and Cr-rich $M_{23}C_6$-type carbides. Toward the end, a phenomenological model was employed to correlate the FCP rates at cycle/time-dependent FCP domain. All the results suggest that an environmental factor, the stress assisted grain boundary oxygen embrittlement (SAGBOE) mechanism, is mainly responsible for the accelerated time-dependent FCP rates of INCONEL 617 and HAYNES 230.

DOI: 10.1007/s11661-011-0877-7

I. INTRODUCTION

THE Next Generation Nuclear Plant (NGNP) program envisions the use of a very high-temperature reactor (VHTR) concept involving a modular high-temperature gas-cooled reactor, using helium as a coolant and a closed-cycle gas turbine to generate electricity and hydrogen without the production of greenhouse gases.[1–3] The reactor core outlet temperature or the turbine inlet temperature has been recommended to be in the range of 1033 K to 1223 K (760 °C to 950 °C) to obtain the highest efficiency possible for power and hydrogen production while maintaining the stability of structural metallic materials. The intermediate heat exchanger (IHX) will be a critical component of the NGNP system that transfers heat from the primary reactor helium coolant to a secondary working fluid, which may include impure helium, an argon/nitrogen gas mixture, or superheated steam with slight potential of oxidization (in the case of a Rankine cycle).[1–3] During operation, the IHX in the VHTR system will be subjected to combined thermal static and cyclic loading (or so-called creep-fatigue loading conventionally), resulting from the synergistic effect of high-temperature environment and temperature-induced repeated or alternating stress. Thus, the consequence of static and cyclic loading interaction (creep-fatigue loading) must be addressed in the selection of materials prior to the design of high-temperature structural components such as heat exchangers. In the NGNP program, the high-temperature design methodology (HTDM) considering environment-induced crack initiation and crack propagation based on fracture mechanics will be considered to design and assess the system life expectancy. Therefore, the high-temperature, low-cycle fatigue life

LONGZHOU MA, Research Scientist, is with the Harry Reid Center for Environmental Studies, University of Nevada—Las Vegas, Las Vegas, NV 89154-4009. Contact e-mail: lma@unlv.nevada.edu SHAWOON K. ROY, Graduate Student, is with the Harry Reid Center for Environmental Studies, University of Nevada—Las Vegas, and is also with the Department of Mechanical Engineering, University of Nevada—Las Vegas. MUHAMMAD H. HASAN, formerly Post-Doctorate with the University of Nevada—Las Vegas, is now Assistant Professor with the Department of Mechanical Engineering, Taibah University, Kingdom of Saudi Arabia. JOYDEEP PAL, formerly Post-Doctorate with the University of Nevada—Las Vegas, is now Lead Engineer with General Electric, Bangalore 560066, India. SUDIN CHATTERJEE, formerly PhD Student, Department of Mechanical Engineering, University of Nevada—Las Vegas, is now Researcher with RD&T, Tata Steel Ltd, Jamshedpur 831003, India.

Manuscript submitted January 28, 2011.
Article published online September 16, 2011

and crack propagation behavior will be thought as important factors for materials evaluation and reactor licensing process.[4]

Ni-based superalloys have been used widely for high-temperature components in the nuclear reactor, gas turbine, and oil refinery system because of their combination of high-temperature strength and oxidation resistance. In general, Ni-based superalloys can be categorized into two groups: precipitation-strengthened and solid-solution-strengthened alloys. The precipitation-strengthened superalloys, like INCONEL 718 and 783 (Special Metals Corporation Family of Companies), are strengthened by Ni_3AlTi-type γ' phase and are creep resistant. Such high-strength, precipitation-strengthened superalloys usually display the time-dependent fatigue crack propagation (FCP) behavior at temperature ranges of 823 K to 993 K (550 °C to 720 °C) in air, *i.e.,* the FCP rate (da/dn) remarkably accelerates when the frequency is decreased below a certain value or when a certain period of hold time is imposed at the maximum load of a fatigue cycle. These temperatures allow the stress state of the crack tip to be defined by a linear elastic fracture mechanics (LEFM) parameter, stress-intensity-factor (K). The enhanced time-dependent FCP rate is associated with intergranular fracture during crack propagation.[5–7] Conventionally, the hold time fatigue, also known as creep-fatigue, can produce the time-dependent FCP behavior, which is thought to be resulted from accumulation of creep and fatigue damage in the stressed crack tip. However, such a creep-fatigue-interaction mechanism is usually applicable for the creep-ductile materials such as Cr-Mo and Cr-Mo-V steels.[8,9] For high-strength Ni-based superalloys, the experimental results demonstrate that the environmental factor, stress assisted grain boundary oxygen embrittlement (SAGBOE) mechanism, plays a predominant role in determining the time-dependent FCP rate in air, and the mechanistic parameter is negligible. The conventional mechanistic creep-fatigue crack propagation model, which simply superposes the cyclic (fatigue) and static (creep) components of crack increment as the total crack growth in one cycle, is not sufficient to represent the time-dependent FCP rate of high-strength superalloys.[5–7,10–13] Indeed, at these temperature ranges wherein K is sufficient to characterize the stress state of crack tip, the conventional term, creep-fatigue crack growth, is misleading.[5–7] Therefore, hold-time fatigue should be a proper term instead of creep-fatigue, provided that the LEFM parameter is valid in front of crack tip. For precipitation-strengthened, high-strength superalloys such as INCONEL 718 and 783, a fully time-dependent FCP model considering oxygen grain boundary diffusion kinetics, oxygen thermal activation energy, and LEFM has been established experimentally to characterize the time-dependent FCP process.[5–7] According to this model, if the FCP rate (da/dn) at the fully time-dependent condition can be correlated with the static crack growth rate (da/dt) under a sustained loading condition, then the environmental effect, or SAGBOE mechanism, would be thought to be responsible for the crack propagation process. The SLCG rate (da/dt) can be characterized by a thermodynamic equation, the Arrhenius equation, wherein the characteristic value of thermal activation energy (Q) evidently indicates the oxygen interaction with materials during crack propagation.

Compared with the precipitation-strengthened superalloys, the solid-solution-strengthened Ni-based superalloys such as INCONEL 617 and HAYNES 230 (Haynes International, Inc., Kokomo, IN) are less creep resistant but have a combination of good high-temperature strength and premier oxidation behavior.[14–16] The FCP behavior of INCONEL 617 and HAYNES 230 under the hold time fatigue or creep-fatigue condition is a major concern to employ HTDM for IHX design in the NGNP system. The identification and understanding of hold time effects on FCP behavior at increased temperature will ensure the reliability and service life expectancy for IHX components.[14] As a prime candidate material for the NGNP system, the low cycle fatigue life and FCP behavior under cyclic and hold time fatigue conditions of INCONEL 617 has been well studied. Nonetheless, the modeling characterization of the complete FCP process of INCONEL 617 at increased temperatures is unavailable.[4,17–19] As a back-up material of INCONEL 617, initial investigations of the fatigue and static crack propagation behavior of HAYNES 230 have been conducted using stress-intensity factor (K) and the change of energy input rate parameter (C_t) at high temperatures ranging from 1073 K to 1200 K (800 °C to 927 °C). However, no literature data exist on the systemic comparison of the FCP behavior of both alloys under both cyclic and hold time fatigue conditions at increased temperature ranges.[20–22]

In this study, crack propagation tests under cyclic fatigue, hold time fatigue, and sustained loading conditions were performed on INCONEL 617 and HAYNES 230 to explore the crack propagation behavior using compact-tension (CT) specimens in air at 873 K, 973 K, and 1073 K (600 °C, 700 °C, and 800 °C) under a constant K-controlled mode. The time-dependent FCP behavior of the experimental alloys was identified and their FCP rates were compared. The fracture surface morphologies associated with crack propagation behavior were characterized by SEM. Similar to the precipitation-strengthened superalloys, a semiempirical mode, based on a thermodynamic equation, was employed to characterize the FCP process of experimental alloys under both cyclic and hold time fatigue conditions.

II. MATERIAL AND EXPERIMENTAL PROCEDURE

A. *Materials*

Rectangular bars of the experimental alloys INCONEL 617 and HAYNES 230 were procured from the Huntington Alloys Corporation (Huntington, WV), and Haynes International, Inc., respectively. Both alloy bars were subjected to the standard solid-solution treatment at a temperature of 1448 K (1175 °C) for INCONEL 617 and 1510 K (1237 °C) for HAYNES 230 followed by rapid cooling. Such thermal treatment is known to

produce isotropic austenitic grains with annealed twins in Ni-based superalloys.[15,16] The chemical composition of these alloys is given in Table I.

B. *Crack Propagation Experiments*

The CT specimens used in the crack-propagation-rate (CPR) test were fabricated from the as-received bar materials in such a way that the crack plane was perpendicular to the short-transverse direction. The American Society for Testing and Materials (ASTM) Designation E 647-2000 standard was followed to prepare the CT specimens. The dimensions of a CT specimen are illustrated in Figure 1. Prior to the CPR test, the CT specimens were precracked up to a length of 2.00 mm in an Instron servo-controlled hydraulic test machine (Instron, Norwood, MA) at room temperature at a load ratio (R = minimum load, K_{min}/maximum load, K_{max}), a frequency, and a maximum stress intensity factor of 0.1, 1 Hz, and 22 MPa$\sqrt{m}$, respectively. A direct-current-potential-drop (DCPD) technique was used to monitor the crack length of the CT specimens continuously during both precrack and CPR tests. The DCPD method involved passing a constant current of 300 mA through the cracking specimen and detecting the voltage drop across the crack mouth caused by the extension of crack length using Johnson's equation,[23] which is given by Eq. [1].

$$\frac{V_i}{V_o} = \frac{\cosh^{-1}\left[\frac{\cosh(\pi y/W)}{\cos(\pi a_i/W)}\right]}{\cosh^{-1}\left[\frac{\cosh(\pi y/W)}{\cos(\pi a_o/W)}\right]} \quad [1]$$

where V_o and a_o are the initial crack mouth potential and crack length, V_i and a_i are the instantaneous crack mouth potential and crack length, y is the half of the distance between the two points for which the crack mouth potential is measured, and W is the specimen width. The stress intensity factor K was obtained using Tada's equation[24]

$$K = \frac{P}{B\sqrt{W}} \cdot \frac{(2 + a/W)}{(1 - a/W)^{\frac{3}{2}}} \cdot \left[0.886 + 4.64(a/W) - 13.32(a/W)^2 + 14.72(a/W)^3 - 5.6(a/W)^4\right] \quad [2]$$

where P is the applied load, B is the specimen thickness, a is the crack size for a CT specimen, and W is the specimen width. Also, $\Delta K = K_{max} - K_{min}$, where K_{max} and K_{min} are the maximum and minimum stress intensity factor, respectively.

Fatigue crack propagation (FCP) and sustained loading crack growth (SLCG) tests were performed at temperatures of 873 K, 973 K, and 1073 K (600 °C, 700 °C, and 800 °C). A ceramic-lined split furnace, which was attached to the Instron test machine, was used to heat the CT specimens to the desired testing temperatures. Figure 2 illustrates the FCP testing procedure. At the testing temperature, a precracked CT specimen was subjected first to a triangular 3-second fatigue allowing a crack length growth of 2.00 mm minimum so that a steady FCP rate could be determined. After the 3-second fatigue test, a series of hold time FCP tests were performed by superimposing various hold times of 60, 120, 300, 600, and 1000 seconds at maximum load of the triangular waveform. Crack extensions ranging from 1.50 to 2.00 mm between each hold time was selected to monitor the instantaneous crack length as a function of the loading cycle at each testing temperature to measure FCP rate, da/dn.

Table I. Chemical Compositions of the Tested Materials (Weight Percent)

Materials	C	Mn	Fe	Si	Cr	Ni	Al	Ti	Co	Mo	W
Alloy 617	0.06	0.12	0.002	—	22.10	54.80	0.87	0.29	12.17	9.52	0.001
Alloy 230	0.11	0.50	0.42	0.39	22.01	60.76	0.40	0.29	0.10	1.25	14.06

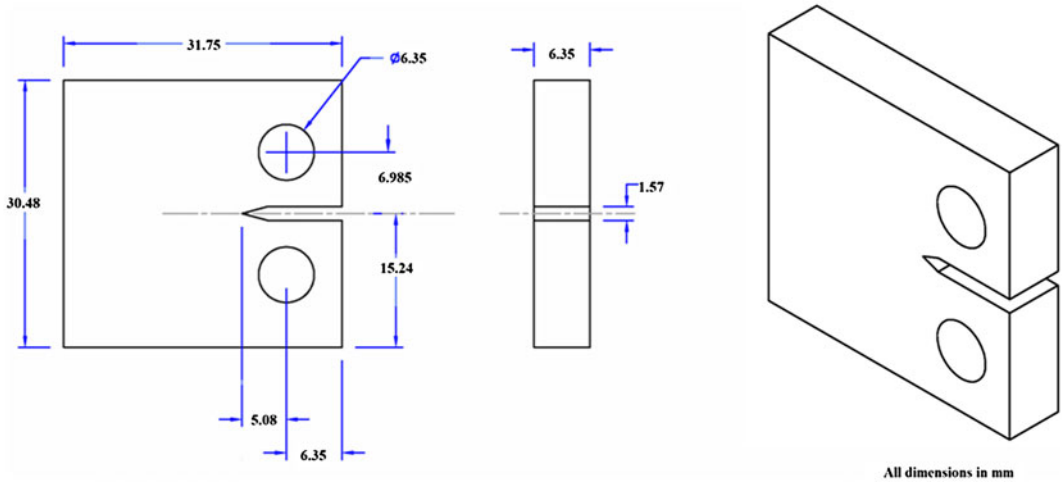

Fig. 1—Geometry of a compact-tension specimen (mm).

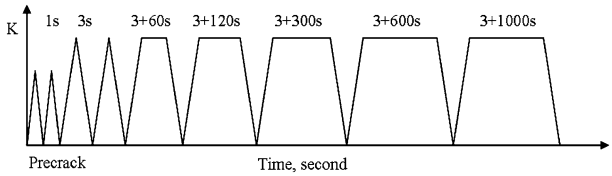

Fig. 2—Schematic illustration of FCP testing procedure.

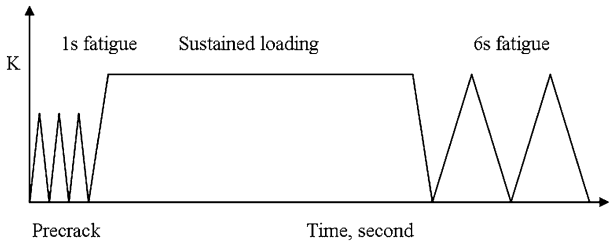

Fig. 3—Schematic illustration of SLCG testing procedure.

During FCP testing, the maximum stress intensity factor (K_{max}) and load ratio (R) were kept at 27.75 MPa$\sqrt{m}$ and 0.1, respectively, so that fatigue crack propagated at a constant ΔK with value of 25 MPa$\sqrt{m}$, which is approximately less than one quarter of fracture toughness of INCONEL 617 and HAYNES 230 at room temperature.[15,16]

In addition to triangular and hold time FCP tests, SLCG tests were conducted also. Figure 3 shows the testing procedure, involving loading a precracked specimen at a constant K with a value of 27.75 MPa$\sqrt{m}$, equal to the K_{max} of the FCP test, for a sufficient period at respective increased temperatures to measure the SLCG rate, da/dt. After the steady SLCG test, the tested specimen was cooled to room temperature and a FCP test with a load ratio (R) of 0.1, a cyclic period of 6 seconds, and K_{max} of 27.75 MPa$\sqrt{m}$ was subsequently carried on the specimen again to identify and measure the damaged zone caused by the previous SLCG. The damage zone concept and the measurement procedure were reported elsewhere.[5–7,24] Mathematically, the sustained loading (or called infinite holding) status can be considered as a specific hold time fatigue with only one cycle, wherein the hold time is sufficiently long. A software program provided by the Fracture Technology Associates (Bethlehem, PA) was used to monitor cracking and record data continuously, which led to the development of crack length *vs* number of loading cycles, and ΔK controlling.

After crack propagation testing, the specimens were broken into two halves to check the beach marks associated with various testing conditions for the crack length and K-value calibration. The DCPD monitor system in this study has a measurement error of 5 to 8 pct. Fractographic evaluations, showing the morphology of failures and cracking of the tested specimens, were performed using a JEOL-5610 SEM (JEOL Ltd., Tokyo, Japan). Optical microstructures of the as-received materials, INCONEL 617 and HAYNES 230, were examined in a polished and etched condition by using a Leica optical microscope (Leica Microsystems Inc., Buffalo Grove, IL). The etchant used was Kalling's reagent, which is a mixture of 40 mL distilled water (H_2O), 40 mL hydrochloric acid (HCl), 40 mL ethanol (CH_3COOH), and 2 g cupric chloride ($CuCl_2$). In addition to crack propagation tests, the tensile properties and hardness of experimental alloys were also measured at room temperature.

III. RESULTS

A. *Microstructure and Tensile Properties*

The microstructures of as-received INCONEL 617 and HAYNES 230 are presented in Figure 4. The optical micrographs of both materials exhibited isotropic microstructure including a few annealed twin structures after solid-solution treatment and lots of carbides distributed along the inter/intra-granular areas (Figures 4(a) and (b)). The grain size measurement indicated that INCONEL 617 and HAYNES 230 had an average grain size of 97 (ASTM No. 4) and 55 μm (ASTM No. 5.5), respectively. Both INCONEL 617 and HAYNES 230 are composed of a face-centered cubic austenite with different types of carbides, which usually form during thermomechanical processing. The major carbide in INCONEL 617 is the Cr-rich $M_{23}C_6$-type nanoscaled carbides.[25,26] Relative to INCONEL 617, HAYNES 230 has higher carbon content (0.11 wt pct) in this study and includes two types of carbides, the primary W-rich M_6C-type and the secondary Cr-rich $M_{23}C_6$-type carbides. In general, the M_6C-type carbide is micron sized and the $M_{23}C_6$-type carbide is nano sized in solid-solution-treated HAYNES 230.[27,28] The SEM examination of only polished as-received materials can reveal the morphology of M_6C-type carbide. Figures 4(c) and (d) presented the SEM micrographs of polished as-received materials, showing that HAYNES 230 includes numerous micron-sized M_6C-type carbides (5 to 6 μm), which, however, are absent in INCONEL 617. The tensile properties and hardness of both materials at room temperature are given in Table II, indicating that INCONEL 617 has slightly higher tensile strength and elongation than HAYNES 230 at room temperature.

B. *Fatigue Crack Propagation*

As examples, the constant ΔK-controlled FCP curves of INCONEL 617 and HAYNES 230 tested at 873 K (600 °C) for 3-second cyclic fatigue and hold time fatigue with various holding periods are presented in Figures 5(a) and (b), respectively. The variations of crack length (a) with number of fatigue cycles (n) under all tested conditions exhibit a linear relationship, indicating that the crack propagated at a constant rate under constant ΔK-controlled mode. The slope of crack growth curve represents the FCP rate, da/dn. Among the hold times with sufficient period, Figure 5 indicates that the FCP rates of both INCONEL 617 and HAYNES 230 increase with the hold time periods. The enhancement of FCP rates of INCONEL 617 are not pronounced for the short hold times such as 60, 120, and 300 seconds, whereas HAYNES 230 shows significant

increase in FCP rates at those hold time periods. All data of crack growth length *vs* fatigue cycle under different temperature and hold time conditions were processed using a linear regression analysis to calculate the FCP rates, which were plotted in Figure 6 as a function of the fatigue period. Both INCONEL 617 and HAYNES 230 exhibit the time-dependent behavior, *i.e.,* the FCP rate, da/dn, is a function of the hold time length. Such time-dependent FCP behaviors have been observed also in many Ni-based superalloys such as INCONEL 718, 783, and Waspaloy.[5–7,11] Considering experimental data scattering, the degree of time dependence at a given temperature increases gradually with the length of hold time, although it may not be significant for INCONEL 617 at short hold time period. Theoretically, a linear relationship between the FCP rate and hold time length can be established when the hold time exceeds a critical value, *i.e.,* FCP becomes fully time dependent.[8] Temperature is an important parameter to affect the time-dependent FCP process. The enhancement of temperature allows the time-dependent FCP to start at a shorter hold time or period, resulting in higher FCP rate. For both INCONEL 617 and HAYNES 230 at 1073 K (800 °C), the time-dependent FCP behavior already started at hold time of 60 seconds. However, for INCONEL 617 at 973 K (700 °C), the time-dependent FCP behavior has not been observed until the length of hold time was 120 seconds. All the data of the crack length *vs* cycle at different temperatures display the linear relationship, suggesting that the LEFM parameter (K) is sufficient to define the stress state of the crack tip at the experimental temperatures.[7] It should be noted that at the highest testing temperature such as 1073 K (800 °C), the crack length variation could not even be measured for hold times of 300 and 1000 seconds because crack advancement was too fast to be recorded by the system. Another interesting observation in Figure 6 is that at 3 seconds cyclic fatigue without holding, INCONEL 617 and HAYNES 230 have comparable FCP rates at temperatures of 873 K and 973 K (600 °C and 700 °C), suggesting that 3-second triangular fatigue at those temperatures allows the crack to propagate in cycle-dependent mode, in which the FCP rates are determined mainly by the mechanistic parameter ΔK. With introduction of hold

Table II. Tensile Properties and Hardness of INCONEL 617 and HAYNES 230

Materials	YS (MPa)	UTS (MPa)	EL (pct)	RA (pct)	Hardness (RB)
Alloy 617	371	855	78.4	62.0	86.8
Alloy 230	361	820	46.0	43.0	92.0

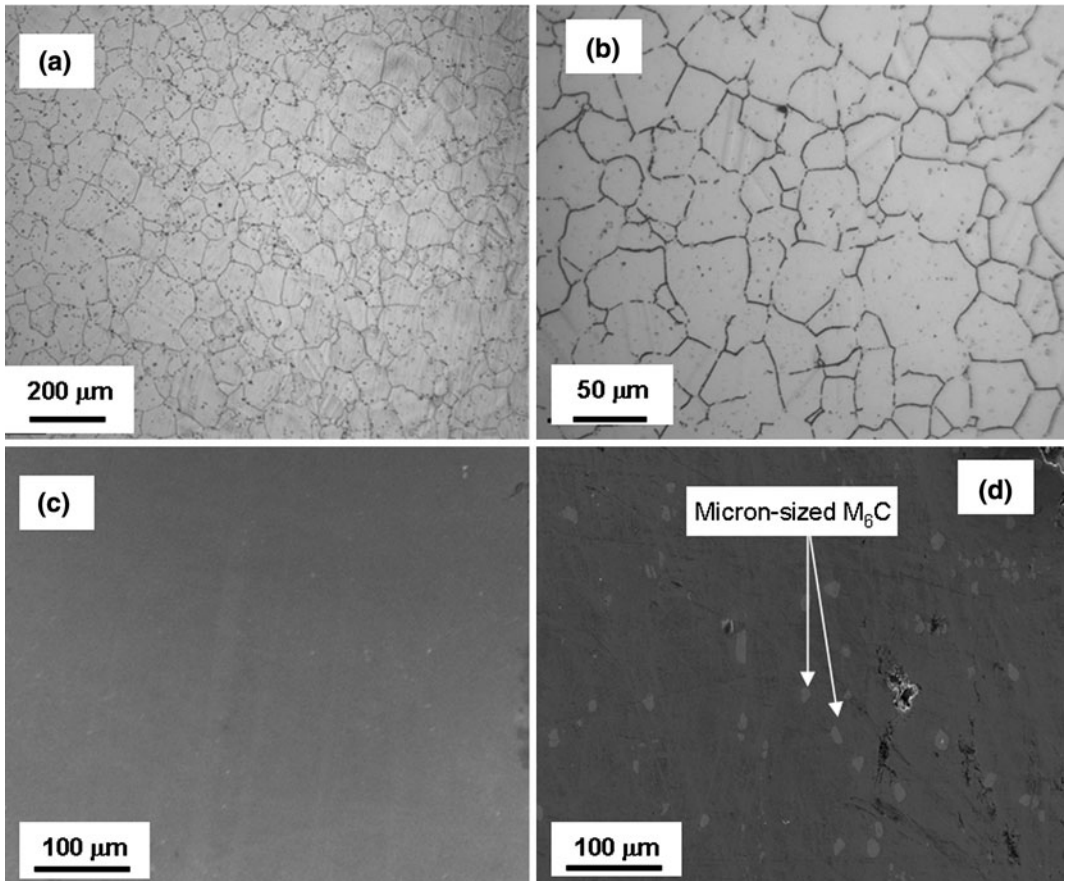

Fig. 4—Microstructures of as-received materials: (*a*) optical micrograph of INCONEL 617, (*b*) optical micrograph of HAYNES 230, (*c*) SEM micrograph of INCONEL 617, and (*d*) SEM micrograph of HAYNES 230.

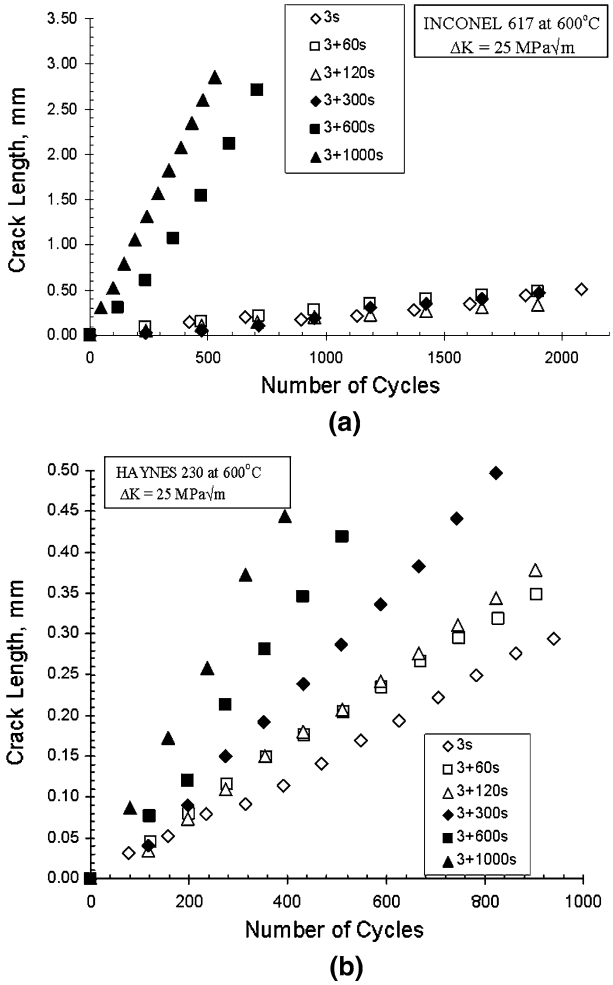

Fig. 5—Constant-ΔK FCP curves for different hold times tested at 873 K (600 °C) in air: (*a*) INCONEL 617 and (*b*) HAYNES 230.

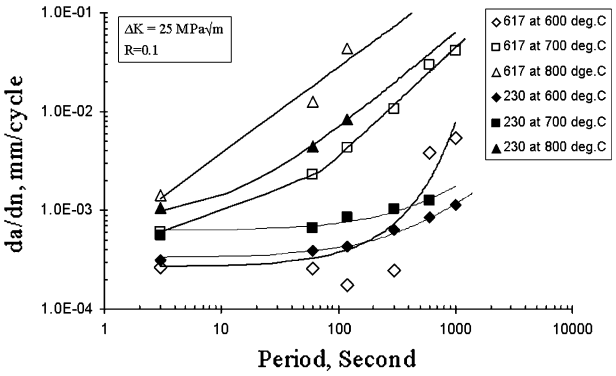

Fig. 6—FCP rates as a function of period at various temperatures.

time, fatigue crack propagates in time-dependent mode, in which the FCP rate becomes a function of ΔK, temperature, and hold time. In summary, the all above experimental results demonstrate that the FCP rates of INCONEL 617 are almost 1-2 magnitudes higher than HAYNES 230 in time-dependent FCP stage, as well as INCONEL 617 starts the time-dependent FCP at shorter hold time than HAYNES 230, suggesting that

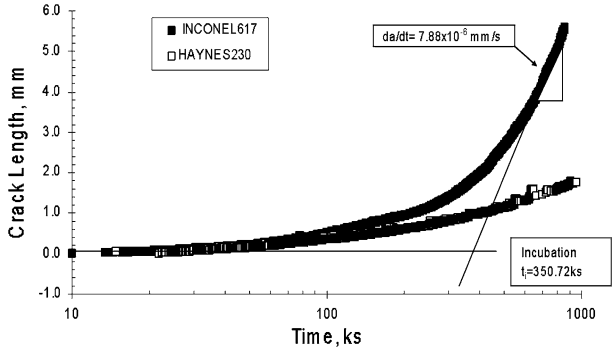

Fig. 7—SLCG of INCONEL 617 and HAYNES 230 in air at constant K equal to 27.75 MPa√m.

HAYNES 230 has higher resistance to time-dependent FCP than INCONEL 617.

C. *Sustained Loading Crack Growth*

The SLCG rate (da/dt) was measured at temperatures of 873 K, 973 K, and 1073 K (600 °C, 700 °C, and 800 °C) following the testing procedure shown in Figure 3. As examples, the SLCG curves for INCONEL 617 and HAYNES 230 at 973 K (700 °C) are shown in Figure 7. For INCONEL 617, initially there is no crack extension for approximately 30,000 seconds after a precracked specimen received a static load K_{max}. At approximately 40,000 seconds, the crack started to initiate and grow. It took approximately 350,000 seconds to reach the steady crack growth. As the sustained load K_{max} was kept constant during crack growth, the crack length has a linear relationship with time. The slope of the linear portion of the crack growth curve in Figure 7 represents the SLCG rate (da/dt). As shown in Figure 7, the intersection between crack growth line and horizontal line represents the incubation (t_i), wherein the crack starts to propagate stably. Figure 7 also shows that HAYNES 230 displays a lower crack growth rate than INCONEL 617. After the completion of SLCG test, the damage zone identification test was conducted subsequently involving an FCP test with the same specimen at room temperature with the same K_{max} as SLCG, 6-second period, and R value of 0.1. The FCP curves of both INCONEL 617 and HAYNES 230 for damage zone tests were plotted as shown in Figure 8, where the FCP exhibits considerably different crack propagation behavior compared with the normal linear steady FCP behavior shown in Figure 5. Because K_{max} was kept the same as the SLCG test, the fatigue crack propagated immediately without any fatigue incubation caused by the plastic zone. The zero cycle refers to the end of the SLCG test. The crack length represents the crack increment at 6-second fatigue. Initially, the fatigue crack grew at a fast rate, and then the growth rate slowed down gradually with the increase of crack length. Eventually, the crack growth rate returned to a stable value and the crack propagated again, showing a linear relationship between the crack length and number of cycles. The distance from the end of SLCG test to the beginning of a normal crack growth rate is defined as

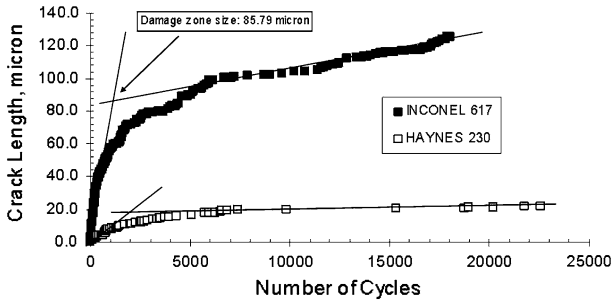

Fig. 8—FCP curves of INCONEL 617 and HAYNES 230 at K_{max} = 27.75 MPa√m, R = 0.1, and room temperature after SLCG testing at 973 K (700 °C).

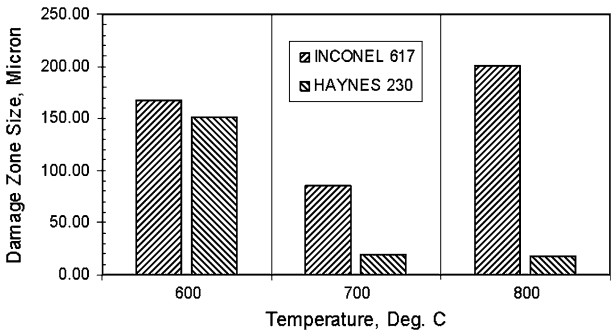

Fig. 9—Damage zone size measurement.

damage zone, inside which the FCP rate was accelerated. As shown in Figure 8 for INCONEL 617, the intersection between the fitting lines of accelerated and normal FCP portion could determine the size of damage zone formed during SLCG. For SLCG at 973 K (700 °C), both INCONEL 617 and HAYNES 230 produced the damage zone with the size of 85.79 and 19.01 μm, respectively. The existence of a damage zone ahead of the crack tip was observed also in other Ni-based, precipitation-strengthened superalloys (such as INCONEL 718 and 783), and it was thought to be the essential mechanism for the time-dependent FCP behavior of those alloys.[5–7]

All data of SLCG tests at different temperatures were processed according to the methods illustrated in Figure 7 and Figure 8 to calculate da/dt, t_i, and the damage zone size. Figure 9 compares the damage zone size of INCONEL 617 and HAYNES 230 after SLCG tests. Early studies indicated that the damage zone is a function of holding period, temperature, and applied load.[5,7,29] Given the testing temperature, Figure 9 shows that HAYNES 230 has smaller damage zone size than INCONEL 617. Figures 10 and 11 illustrate the plots of the incubation (t_i) *vs* temperature, and the SLCG rate (da/dt) as a function of absolute temperature inverse ($1/T$), exhibiting that a high value of da/dt and low value t_i are observed at a higher temperature. For da/dt *vs* $1/T$ in Figure 11, the well-defined linear relationship was noticed. Therefore, a thermodynamic equation, the Arrhenius equation, was employed to correlate the da/dt and temperature as shown in Eq. [3]. Figure 11 indicates also that HAYNES 230 has one

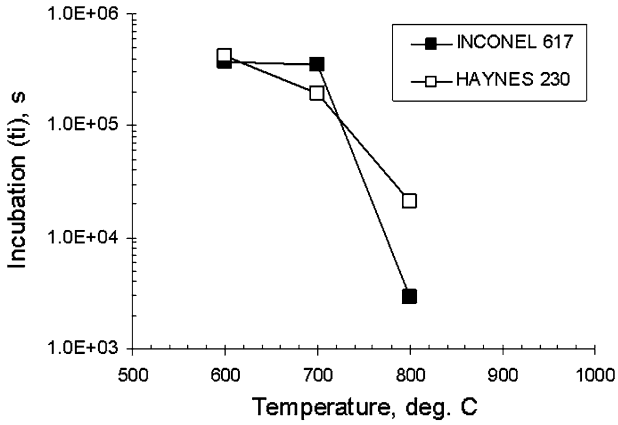

Fig. 10—Incubation *vs* temperature (°C).

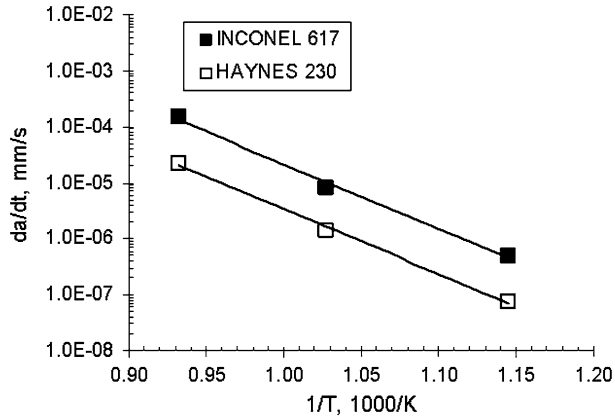

Fig. 11—SLCG rate, da/dt, *vs* $1/T$.

order of magnitude lower da/dt than INCONEL 617, suggesting HAYNES 230 has higher resistance to SLCG. The rate of SLCG can be expressed as

$$\frac{da}{dt} = \mathrm{C} \cdot e^{\left(\frac{-Q}{RT}\right)} \qquad [3]$$

where C is a constant, T is the absolute temperature, R is the gas constant, and Q is a type of thermal activation energy. Based on Figure 11, the Q value can be calculated as 222.15 kJ/mole for INCONEL 617 and 221.75 kJ/mole for HAYNES 230, respectively. For the precipitation-strengthened, Ni-based superalloys INCONEL 718 and 783 at K_{max} equal to 26.5 and 35 MPa√m, the Q values have been reported to be 255 and 242 kJ/mole for SLCG in air, respectively.[5,7,29] The activation energy of 232 kJ/mole has been reported for the oxidation of HAYNES 230 in stress-free state at high temperatures.[30] The measured Q value in Figure 11 suggests the SLCG process of INCONEL 617, and HAYNES 230 is a rate-controlling process including oxygen thermal interaction with materials. It was thought that the applied stress at the crack tip could assist oxygen interaction with material of crack area through reducing the effective activation energy.[31] Therefore, it is not surprising that the activation energy

measured from SLCG of HAYNES 230 is approximately 10 kJ/mole lower than that measured from high-temperature oxidation in stress-free state.

IV. DISCUSSION

A. *Fractography*

As illustrated previously, the experimental results indicated that both INCONEL 617 and HAYNES 230 displayed the time-dependent FCP behavior under the hold time fatigue condition. The time-dependent FCP rate increased with the period of hold time. Under sustained loading condition, both INCONEL 617 and HAYNES 230 exhibited the rate-controlling crack growth process. Another interesting result is that HAYNES 230 displayed lower time-dependent FCP rates and SLCG rates than INCONEL 617 (shown in Figures 6 and 11), whereas HAYNES 230 has smaller grain size (55 μm) than INCONEL 617 (97 μm), as shown in Figures 4(a) and (b). Usually, the fine grain size facilitates the time-dependent FCP and SLCG of superalloys, and consequently it reduces the cracking resistance under the time-dependent condition.[22,32,33] To understand these testing results, all specimens were broken into two halves after testing, and SEM fractographic analyses were conducted. The SEM observations of fracture surfaces indicate that the accelerated time-dependent FCP rates caused by an introduction of hold time are associated with fracture mode change. Figure 12 shows SEM micrographs of the fracture surfaces for specimen of INCONEL 617 tested at 973 K (700 °C) under 3 seconds, 3 + 300 seconds, and 3 + 1000 seconds fatigue. At 3-second fatigue (cycle-dependent FCP domain), the crack propagated in a typical transgranular fracture mode and the well-defined fatigue striation structures were observed (Figure 12(a)). When a hold time with period of 300 seconds or 1000 seconds was imposed at K_{max}, the FCP displayed the time-dependent behavior, resulting in the acceleration of the FCP rate. The corresponding fracture appearances showed the intergranular fracture feature in Figures 12(b) and (c). The grain boundary splitting was evident and no fatigue striations appeared on the fracture facets. A few nano-sized voids associated with intergranular $M_{23}C_6$ carbides were observed, suggesting that carbides were pulled out during fracture. Under the sustained loading condition, the crack propagation became fully time dependent in all testing temperatures, and the crack propagated in fully intergranular fracture mode (Figure 13). Facet grain boundaries were split during crack propagation, and some scattered carbides and voids were still found on grain boundaries. A few oxidized features appeared on the grain boundaries and slightly increased with temperature, resulting in rough grain boundary surfaces. The intergranular fracture is the brittle failure mode, suggesting that little grain boundary cohesion occurred during fracture.

Compared with INCONEL 617, the fracture surface of HAYNES 230 tested at a high temperature was

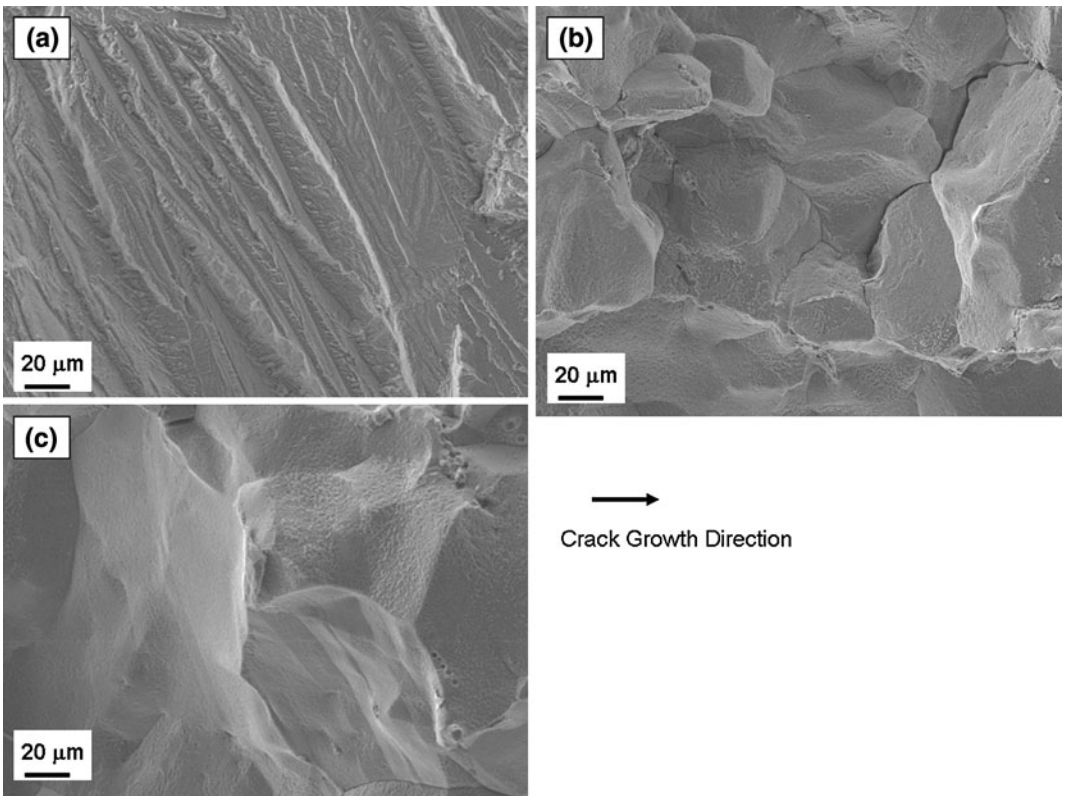

Fig. 12—SEM fracture surface micrographs of INCONEL 617 specimen subjected to FCP tests at 973 K (700 °C): (*a*) at 3 s; (*b*) at 3 + 300 s; (*c*) at 3 + 1000 s.

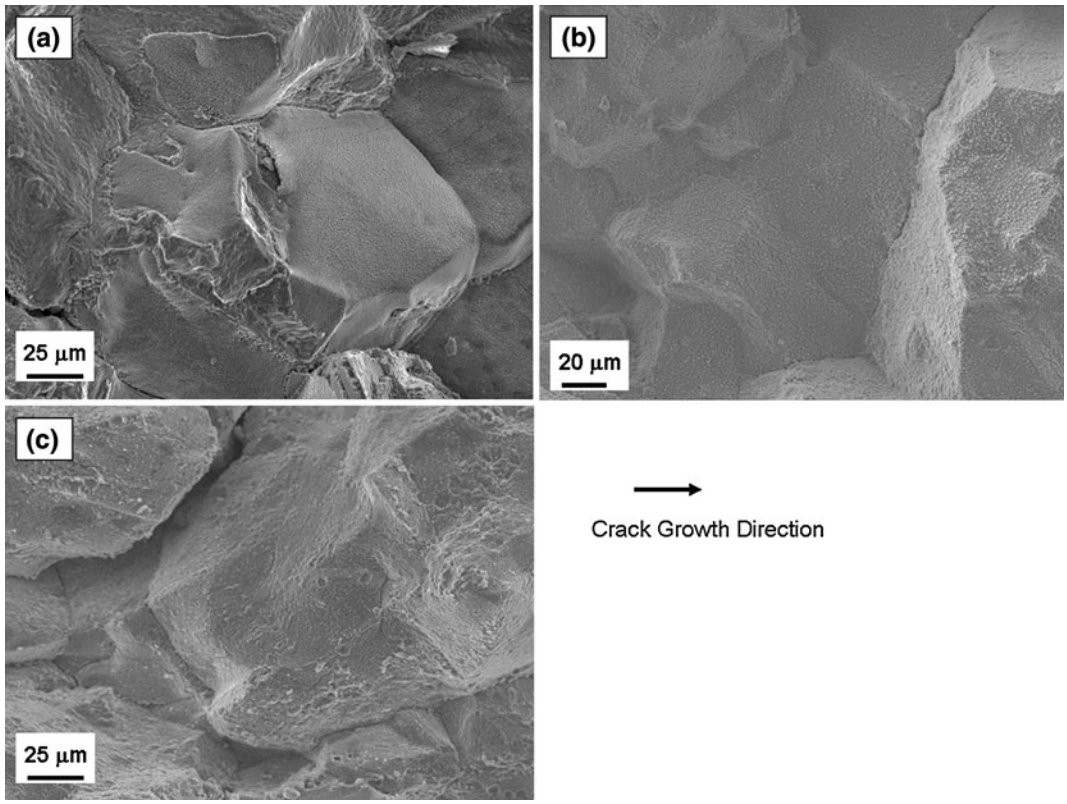

Fig. 13—SEM fracture surface micrographs of INCONEL 617 specimen subjected to SLCG tests: (*a*) at 873 K (600 °C), (*b*) at 973 K (700 °C), and (*c*) at 1073 K (800 °C).

usually covered by dense oxides and carbides, which somewhat suppressed the details of fracture features. Figure 14 shows SEM micrographs of HAYNES 230 tested at 973 K (700 °C) at 3 seconds and 3 + 300 seconds of fatigue. Because of the presence of two types of carbides, micron-sized M_6C and nano-sized $M_{23}C_6$ carbides, the fracture features of HAYNES 230 are remarkably different from that of INCONEL 617. The fracture appearance at 3 seconds fatigue showed the fatigue striations in Figure 14 (a), whereas some areas were covered by oxides. In addition, lots of cleaved micron-sized M_6C-type carbides were noticed, showing the flat and featureless fracture facets as indicated in Figure 14(a). When the crack propagated at 3 + 300 seconds fatigue, the FCP was time dependent and the FCP rate increased. The corresponding fracture surface was relatively rough and cleaved M_6C facets were still visible; however, the fatigue striations disappear and some secondary cracks of the cleaved M_6C-carbides were observed in Figure 14(b). Figure 14(c) shows a close-up view of highlighted area in Figure 14(b), exhibiting that the rough surface is caused by the secondary carbides, the $M_{23}C_6$-type carbides, which are usually in nanoscale size and distributed along grain boundaries in HAYNES 230.[28] So, these dimple-enriched rough surfaces are the intergranular fracture surface indeed. The nano-sized intergranular $M_{23}C_6$ particles could act as nucleation sites of microvoids during grain boundary splitting, producing the dimple rupture (or called microvoid coalescence fracture) features. The micron-sized M_6C-type carbides ahead of the crack were passed by forming the cleavage surface during crack propagation, which sometimes leads to the secondary cracks that may reduce the crack growth rate.[28] Therefore, the fracture mode of HAYNES 230 under the time-dependent FCP condition is combined with dimple-included intergranular fracture together with M_6C-type carbide cleavage and secondary cracks. Figure 15 indicates that lots of cleaved carbides, secondary cracks, and intergranular dimples are present under the SLCG condition at 873 K, 973 K, and 1073 K (600 °C, 700 °C, and 800 °C), suggesting the similar fracture mode as time-dependent fatigue. Therefore, the combination of dimple-included intergranular fracture accompanying with carbide cleavage and secondary cracks are responsible for the lower crack growth rates of HAYNES 230 compared with INCONEL 617 at the condition of time-dependent FCP and SLCG.

B. *Time-Dependent FCP of INCONEL 617 and HAYNES 230*

As illustrated in Figure 5, the FCP rates of INCONEL 617 and HAYNES 230 increase with the period of hold time at an increased temperature under the time-dependent condition. At the fully time-dependent stage, da/dn displays the linear relationship with the period of fatigue. Mathematically, the SLCG rate (da/dt) can be correlated with the time-dependent FCP rate (da/dn) at the fully time-dependent stage because the sustained loading can be considered as a specific hold time fatigue with only one cycle and a prolonged holding period. To

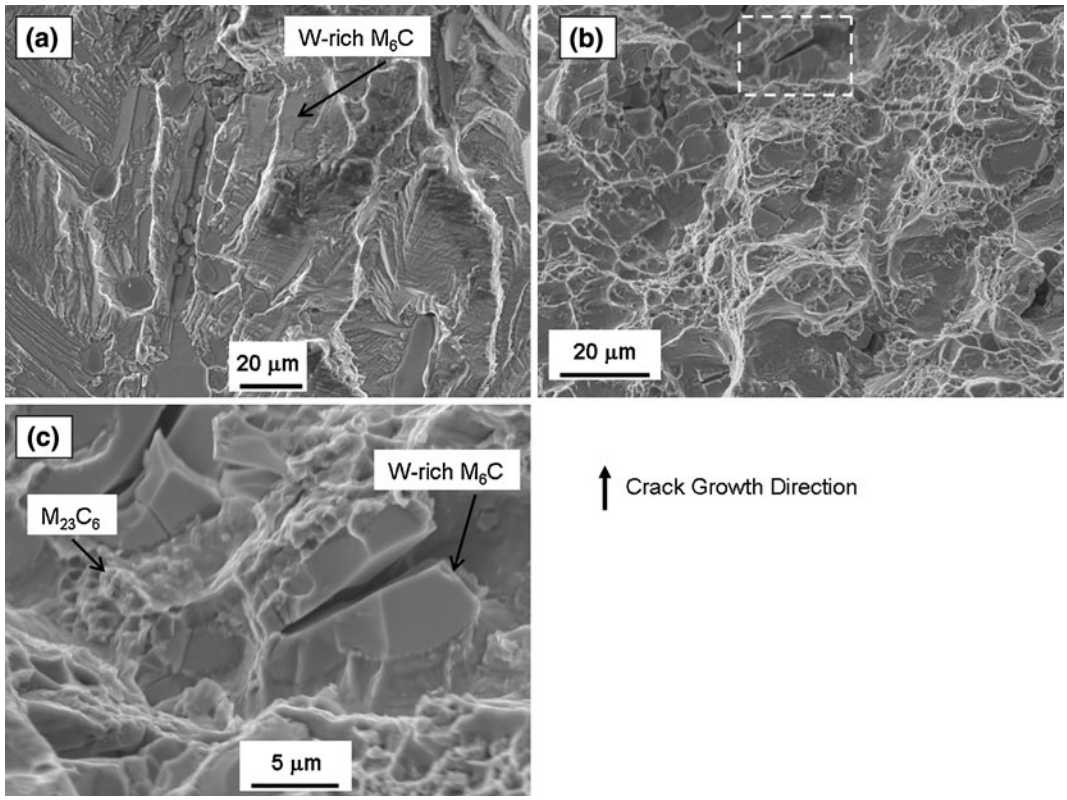

Fig. 14—SEM fracture surface micrographs of HAYNES 230 specimen subjected to FCP tests at 973 K (700 °C): (*a*) at 3 s and (*b*) at 3 + 300 s. (*c*) Close-up view of (b).

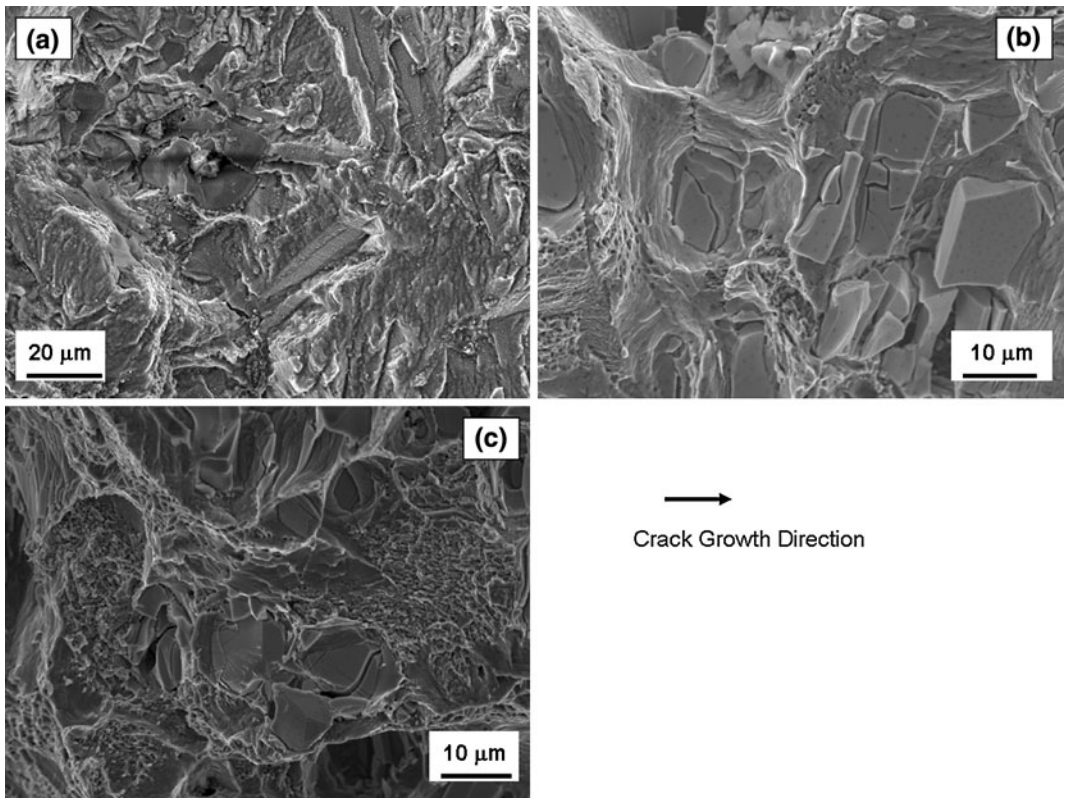

Fig. 15—SEM fracture surface micrographs of HAYNES 230 specimen subjected to SLCG tests: (*a*) at 873 K (600 °C), (*b*) at 973 K (700 °C), (*c*) at 1073 K (800 °C).

identify the fully time-dependent FCP process, the FCP rate (da/dn) was converted into the static crack growth rate (da/dt) by using Eq. [4]

$$\frac{da}{dt} = \frac{1}{t} \cdot \frac{da}{dn} \qquad [4]$$

where t is the fatigue period.

Figure 16 shows the plots of static crack growth rate (da/dt) converted by Eq. [4] using the data in Figure 6 as a function of fatigue period (t). To correlate the SLCG process with the FCP, the infinite period (t_∞) was employed to represent the period of the SLCG condition. Considering the experimental scattering, Figure 16 shows that the static crack growth rate (da/dt) moronically decreases with the period when a fatigue crack grows in the triangular fatigue with 3-second period or hold time fatigue with the short holding periods. This stage is called the cycle-dependent FCP domain, wherein da/dt decreases with the period. In contrast, when the fatigue period increases to a certain value, the static crack growth rate (da/dt) is a constant and equal to the SLCG rate, *i.e.,* da/dt at a period of t_∞. This stage is called fully time-dependent FCP domain, wherein da/dt is independent of the fatigue period and the SLCG rate can be related to the FCP rate. As expected, a high temperature usually causes the higher crack growth rate in cycle/time-dependent FCP stage. It should be noted that the various minimum holding periods are required to approach the fully time-dependent FCP at different temperatures. Decreasing the temperature requires a longer hold time to reach the fully time-dependent FCP stage. For example, HAYNES 230 needs at approximately 20,000 seconds hold to reach the fully time-dependent FCP stage at 873 K (600 °C) (Figure 16(b)). Therefore, the results of Figure 16 as well as the presence of incubation for SLCG suggest that the conventional concept, which considers the hold time FCP rate as superposition of fatigue and creep crack growth rate, seems to be incorrect for the experimental alloys INCONEL 617 and HAYNES 230 in the testing condition where K can define the stress state at the crack tip.

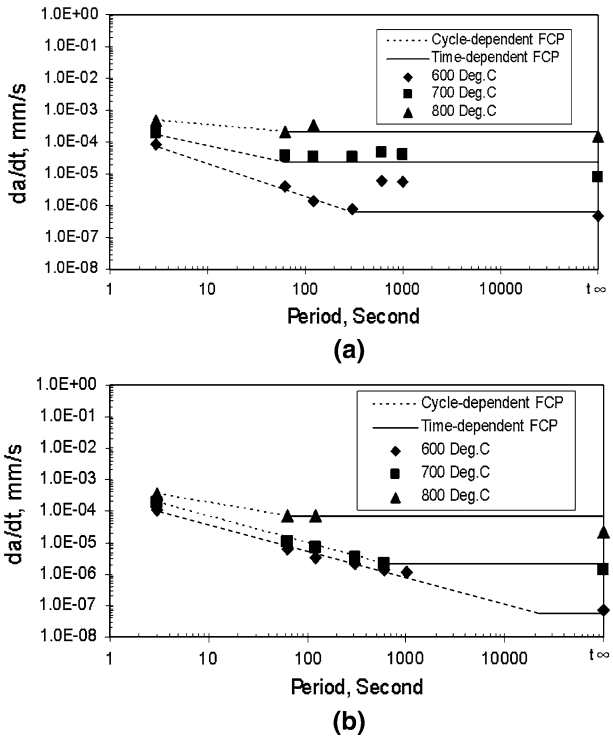

Fig. 16—Static crack growth, da/dt, *vs* period at K_{max} = 27.75 MPA√m: (*a*) INCONEL 617 and (*b*) HAYNES 230.

C. *Crack Propagation Mechanism*

It has been well documented that the accelerated time-dependent FCP rate of precipitate-strengthened Ni-based superalloys caused by the hold time is associated with SAGBOE, which allows the crack to propagate in an intergranular fracture mode.[5,27] A damage zone model based on the SAGBOE mechanism has been proposed to characterize the time-dependent FCP and SLCG process of INCONEL 718 and 783, and the detailed damage zone mechanism can be found in References 5–7 and 26. In this study, the presence of a damage zone has been confirmed in Figure 8, and the measured thermal activation energy for SLCG is relatively lower than that for stress-free high-temperature oxidation of HAYNES 230. Therefore, the time-dependent FCP behavior of INCONEL 617 and HAYNES 230 can be characterized also using the damage zone model. Accordingly, when the specimens of INCONEL 617 and HAYNES 230 were subjected to a hold time fatigue, the oxygen in air was thought to penetrate along the grain boundary at the crack tip and interact with grain boundary materials during holding. As a result, a damage zone ahead of the crack tip was formed. Inside the damage zone, materials have been embrittled because of an oxygen interaction at the grain boundaries. After holding, the following cyclic loading (unloading and reloading) permitted the crack to advance at a fast rate within the damage zone. The crack advancement rate was related to the degree of the damage and damage-zone size, which were a function of applied loading, temperature, and hold time length. Thus, a high-temperature and long holding period usually produce the high FCP rate and promote the time-dependent FCP occurrence. For SLCG as shown in Figure 7, the holding period was extended to a prolonged period. When a precracked specimen was subjected to a sustained loading K_{max} at the testing temperature, the crack could not grow immediately. As time elapsed, oxygen in air was believed to penetrate along the grain boundary to form a damage zone ahead of the crack tip. The damage degree and damage zone size increased with holding time until to a critical value, wherein a crack initiated and then propagated. The duration of damage zone establishment corresponded to the incubation. The steady SLCG rate (da/dt) was equal to the propagation rate of the damage zone and was associated with the damage zone size and damage degree.[5–7,26] When the consumption and formation of the damage zone ahead of crack tip approached the dynamic balance status, the sustained loading crack

propagated at a steady rate. Therefore, as displayed in Figure 9, the fact that HAYNES 230 has a smaller damage zone size than INCONEL 617 is thought to be associated with the lower SLCG rates. Figure 17 shows the FCP curve of damage zone identification test and the corresponding SEM micrograph of fracture surface for INCONEL 617 specimen tested at room temperature and 6-second fatigue subsequently after the completion of SLCG at 1073 K (800 °C). Figure 17(a) demonstrates that INCONEL 617 has an accelerated FCP rate inside the damage zone with size of approximately 201 μm. The corresponding SEM micrograph of fracture morphology exhibits a boundary between SLCG at 1073 K (800 °C) and 6-second FCP at room temperature. In the region of SLCG at 1073 K (800 °C), the fracture feature shows the typical intergranular fracture. In the region of FCP at 6 seconds and room temperature, the fracture mode shows intergranular fracture first and then gradually transforms to the conventional fatigue fracture with transgranular striations. The intergranular fracture area in the 6-second FCP region represents the damage zone formed during the SLCG at 1073 K (800 °C). The FCP rate increased dramatically within the damage zone (Figure 17(a)). As the crack propagated further, the fracture mode transformed gradually to a transgranular fracture accompanying the decrease of the FCP rate. As crack passed the damage zone, the FCP rate resumed as normal and the fracture mode became a fully transgranular mode (Figure 17(b)). The width of the intergranular fracture domain in the 6-seconds FCP region is in agreement with the damage zone size measured in Figure 17(a). For HAYNES 230, the damage zone size is only approximately 21 μm (Figure 18(a)). The fracture feature of damage zone is not clear because of the presence of many cleaved M_6C carbides and oxides. Nonetheless, the transgranular feature from FCP outside the damage zone, the dimple-included intergranular fracture feature from FCP inside the damage zone, and SLCG at 1073 K (800 °C) are still visible (Figure 18(b)). Lots of intergranular dimples are noticed, which indicate the grain boundary damage caused by SLCG. In contrast to INCONEL 617, numerous intergranular carbides in HAYNES 230 may block the oxygen penetration along grain boundaries, resulting in forming a smaller damage zone.

D. *Modeling Characterization of Time-Dependent FCP*

According to the preceding discussion, the time-dependent FCP and SLCG processes are essentially rate-controlling processes associated with the formation and propagation of a damage zone ahead of the crack tip. Therefore, a time-dependent factor, $\alpha(t,T)$, including

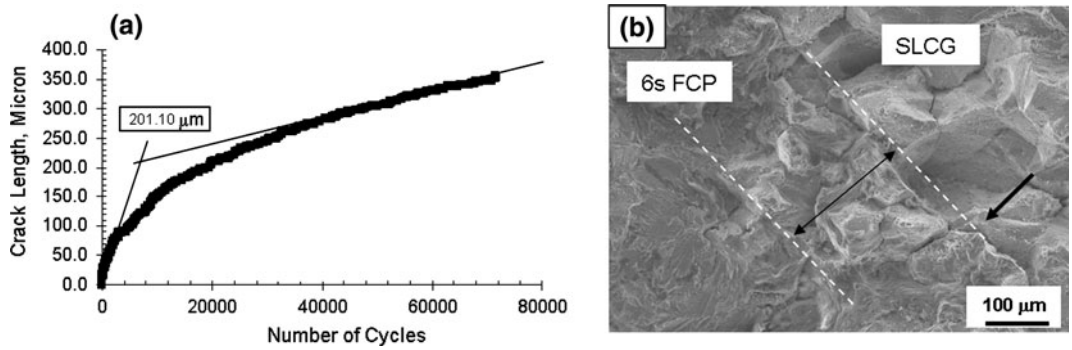

Fig. 17—Damage zone examination of INCONEL 617: (*a*) FCP curve at room temperature after SLCG test at 1073 K (800 °C). (*b*) Corresponding SEM micrograph of fracture surface. The arrow indicates the crack growth direction.

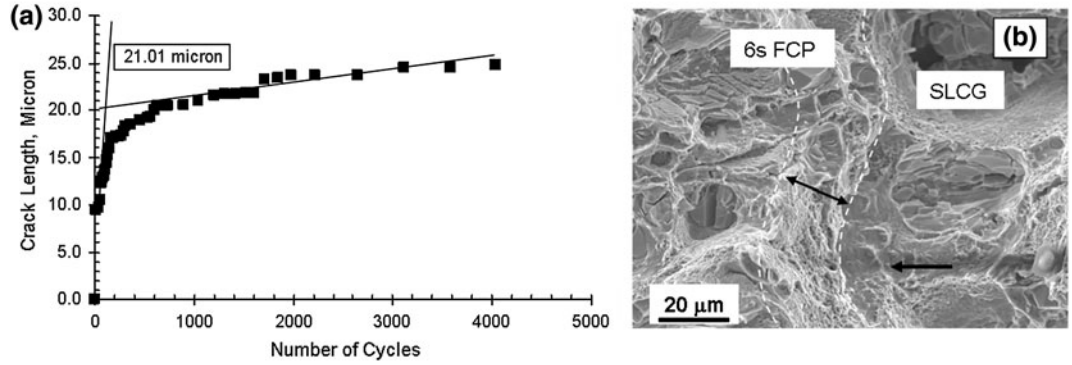

Fig. 18—Damage zone examination of HAYNES 230: (*a*) FCP curve at room temperature after SLCG test at 1073 K (800 °C). (*b*) Corresponding SEM micrograph of fracture surface. The arrow indicates the crack growth direction.

the parameter of thermal activation energy (Q), fatigue period (t), and temperature (T), can be adapted to normalize the all measured FCP rates. The time-dependent factor is defined as

$$\alpha(t,T) = \ln(t) - \frac{Q}{RT} \quad [5]$$

where Q is the thermal activation energy for SLCG, t is the period of fatigue, R is gas constant, and T is the absolute temperature. As indicated in Figure 11, because INCONEL 617 and HAYNES 230 have identical Q values, the average value of 222.00 kJ/mole based on the two experimental alloys was used in Eq. [5]. Figure 19 replots all the measured FCP rates of INCONEL 617 in Figure 6 against the time-dependent factor $\alpha(t,T)$, showing that all data fall in one curve that consists of two straight lines. The horizontal line with a constant FCP rate (da/dn) represents the cycle-dependent FCP stage, where the FCP rate is the pure mechanical behavior associated with material Young's modulus and the cyclic stress intensity factor (ΔK). The other line obtained from the SLCG data represents the time-dependent FCP stage. The crack growth rate is controlled by the static stress intensity factor (K_{max}). The empirical expression of the time-dependent FCP of INCONEL 617 in Figure 19 can be obtained as follows:

$$\ln\left(\frac{da}{dn}\right) = k\alpha(t,T) + B \quad [6]$$

where k and B are constants, respectively.

Similarly, the data of the FCP rates for HAYNES 230 were indexed using $\alpha(t,T)$. The characteristics curves of FCP for INCONEL 617 and HAYNES 230 are exhibited in Figure 20. In cycle-dependent FCP domain, INCONEL 617 and HAYNES 230 have similar FCP rates. Because INCONEL 617 and HAYNES 230 have an identical Young's modulus from room temperature to high temperature,[14,15] it is not surprising that the FCP rates are identical at same ΔK. At the cycle-dependent FCP stage, Paris law can be used to describe the FCP rate as follows:

$$\frac{da}{dn} = A \cdot (\Delta K)^m \quad [7]$$

where A is a constant, ΔK is the cyclic stress intensity factor, and m is a material constant.

For time-dependent FCP of INCONEL 617, the empirical expression is:

$$\ln\left(\frac{da}{dn}\right) = 1.08 \cdot \alpha(t,T) + 19.01 \quad [8]$$

For time-dependent FCP of HAYNES 230, the FCP rate is

$$\ln\left(\frac{da}{dn}\right) = 0.96 \cdot \alpha(t,T) + 14.46 \quad [9]$$

The semi-empirical time-dependent FCP model provides a simple and straightforward method to characterize the complete FCP behavior of INCONEL 617 and HAYNES 230 under both pure fatigue and hold time fatigue conditions. In Figure 20 and Eq. [6], there are two interesting parameters at cycle/time-dependent FCP stage. One is the offset value of the time-dependent factor for the beginning of time-dependent FCP. The other is the degree of time dependence, *i.e.,* the slope (k) in Eq. [6], when crack propagation becomes time-dependent. If the absolute value of time-dependent factor offset and k are lower, then the resistance to time-dependent FCP is higher. In Figure 20, HAYNES 230 has a higher resistance to time-dependent FCP than INCONEL 617. Both the time-dependent factor offset and the k value are parameters of the material property and can be controlled through the modification of alloy chemical composition and microstructures. The characteristics curve indexes the resistance of the alloy to time-dependent FCP. When the time-dependent factor is small, the crack propagates at a cycle-dependent mode and the fracture mode is transgranular. The FCP behavior is related to the mechanical damage process associated with material Young's modulus and ΔK. Hence, the FCP rate is constant under a constant-ΔK condition. As the time-dependent factor increases, the fatigue propagates at a time-dependent mode. The FCP rate no longer remains constant; it increases with the time-dependent factor and is determined by the maximum loading K_{max}, hold time period, and temperature. The intergranular fracture is associated with the crack propagation at the time-dependent domain.

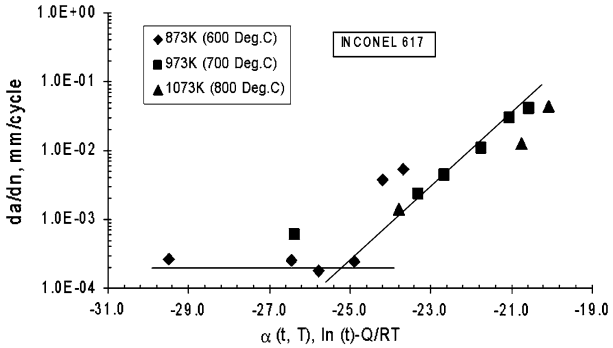

Fig. 19—Normalized FCP rates, da/dn, of INCONEL 617 by the time-dependent factor $\alpha(t,T)$ at K_{max} = 27.75 MPa$\sqrt{m}$.

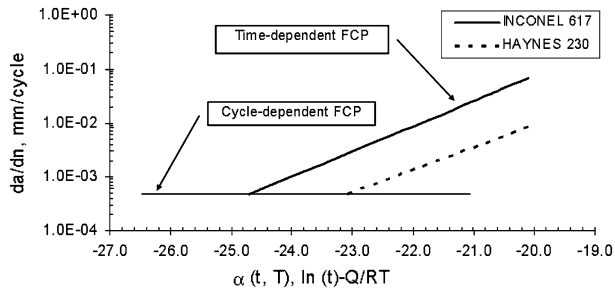

Fig. 20—Characteristic curves to describe the FCP behavior of INCONEL 617 and HAYNES 230.

V. CONCLUSIONS

The effects of temperature and hold time on FCP behavior as well as the SLCG of INCONEL 617 and HAYNES 230 were studied extensively using precracked CT specimens under a constant *K*-controlled mode. The fracture mode was discussed. At a fully time-dependent domain, the FCP rate was related to the SLCG rate. Toward this end, a characteristic curve can characterize all the data. The key results suggest the following conclusions:

1. Both INCONEL 617 and HAYNES 230 can display fully time-dependent FCP behavior at increased temperatures ranging from 873 K to 1073 K (600 °C to 800 °C) if the fatigue period or hold time becomes sufficiently long. The crack propagation rate under a fully time-dependent condition is determined by the static stress intensity factor K_{max}.
2. Both INCONEL 617 and HAYNES 230 display the rate-controlling SLCG process, and a thermodynamic equation can correlate the crack growth rates. Both alloys show the identical thermal activation energy during crack growth.
3. The fracture mode of INCONEL 617 at time-dependent FCP and SLCG is a fully intergranular fracture. Relative to INCONEL 617, the fracture mode of HAYNES 230 under time-dependent condition is the combination of dimple-included intergranular fracture accompanied by carbide cleavage and secondary cracks. Numerous primary M_6C and secondary intergranular $M_{23}C_6$ carbides in HAYNES 230 are responsible for the mixed fracture modes and lower crack propagation rates.
4. A time-dependent factor including thermal activation energy, period, and temperature can be employed to index all data of the experimental alloys. Two characteristic curves are obtained to characterize the FCP process of INCONEL 617 and HAYNES 230 at the cycle and time-dependent FCP domain. HAYNES 230 displays lower time-dependent FCP rates than INCONEL 617.
5. In the experimental temperatures of 873 K to 1073 K (600 °C to 800 °C), the LEFM parameter (*K*) is sufficient to characterize the crack tip stress state. The conventional creep-fatigue mechanism-induced time-dependent FCP seems to be invalid in such temperature ranges, and the hold time fatigue should be a proper term instead of creep-fatigue.
6. Both INCONEL 617 and HAYNES 230 are susceptible to SAGBOE-induced cracking at an increased temperature. However, HAYNES 230 seems to display higher cracking resistance than INCONEL 617. When both alloys are used in highly oxidizing environment such as the NGNP system, the SAGBOE-induced degradation should be considered.

ACKNOWLEDGMENTS

This work was funded by the United States Department of Energy (US DOE), Nuclear Energy University Program under grant No. of DE-AC07-051D141517 and Project No. 00090711. Many thanks are also due to Dr. Richard Wright at Idaho National Laboratory, Idaho Falls, ID, for helpful discussions as well as DOE University of Nevada–Las Vegas Transmutation Research Program for assistance.

REFERENCES

1. W.R. Corwin: *Nucl. Eng. Tech.*, 2006, vol. 38, pp. 591–618.
2. R. Wright, J. Simpson, A. Wertsching, and W.D. Swank: *Proc. 4th International Topical Meeting on High Temperature Reactor Technology HTR 2008*, Washington, DC, 2008, pp. 1–5.
3. R.N. Wright: Report No. INL/EXT-06-11494, Idaho National Laboratory, 2006.
4. T.C. Totemeier and H. Tian: *Mater. Sci. Eng. A*, 2007, vols. 469–470A, pp. 81–87.
5. L.-Z. Ma, K.-M. Chang, S.K. Mannan, and S.J. Patel: *Metall. Mater. Trans. A*, 2002, vol. 33A, pp. 3465–77.
6. K.-M. Chang, M.F. Henry, and M.G. Benz: *JOM*, 1990, pp. 29–35.
7. K.-M. Chang: Report No. 91CRD 066, GE Research & Development Center, 1991.
8. A. Saxsena: *Fatig. Eng. Mater. Struct.*, 1980, vol. 3, pp. 247–55.
9. V. Dimopulos, K.M. Nikibin, and G.A. Webster: *Metall. Trans. A*, 1988, vol. 19A, pp. 873–80.
10. R. Mollins, G. Hochstetter, J.C. Chassaigne, and E.E Anderieu: *Acta Mater.*, 1997, vol. 45, pp. 663–74.
11. S. Floreen: *Metall. Trans. A*, 1975, vol. 6A, pp. 1741–49.
12. S. Floreen and R.H. Kane: *Metall. Trans. A*, 1979, vol. 10A, pp. 1745–51.
13. K. Sadananda and P. Shahinian: *Metall. Trans. A*, 1977, vol. 8A, pp. 439–49.
14. W.J. Ren: *Press. Vessel Tech.*, 2009, vol. 31, pp. 044002/1–15.
15. Special Metals Corporation: Inconel Alloy 617, Publication No. SMC-029, 2005.
16. Haynes International Inc.: HAYNES 230 Alloy, High Temperature Alloys Brochure, Publication No.: H-3024E, 2009.
17. J.K. Benz, J.H. Kim, and R.G. Ballinger: *J. Eng. Gas. Turbines & Power,* 2010, vol. 132, pp. 102901/1–7.
18. S.-S. Hsu: *J. Nucl. Sci. Technol.*, 1993, vol. 30 (4), pp. 302–13.
19. K. Bhanu, S. Rao, H. Schiffers, H. Schuster, and H. Nickel: *Metall. Trans. A*, 1988, vol. 19A, pp. 360–71.
20. Y.L. Lu, P.K. Liaw, Y. Sun, G.Y. Wang, S.A. Thompson, J.W. Blust, P.F. Browning, A.K. Bhattacharya, J.M. Aurrecoechea, and D.L. Klarstrom: *Acta Mater.*, 2007, vol. 55, pp. 767–75.
21. A.K. Roy, S. Chatterjee, M.H. Hasan, J. Pal, and L.-Z. Ma: *Mater. Sci. Eng. A*, 2010, vol. 527, pp. 4830–36.
22. X.Y. Lee, Y.L. Lu, P.K. Liaw, H. Choo, S.A. Thompson, J.W. Blust, P.F. Browing, A.K. Bhattacharya, J.M. Aurrecoechea, and D.L. Klarstrom: *Mech. Time-Depend. Mater.*, 2008, vol. 12, pp. 31–44.
23. H.H. Johnson: *Mater. Res. Stand.*, 1965, vol. 5, pp. 442–45.
24. H. Tata, P. Paris, and G. Irwin: *The Stress Analysis of Crack Handbook*, Del Research Corporation, St. Louis, MO, 1985.
25. T.S. Jo, J.H. Lim, and Y.D. Kim: *J. Nucl. Mater.*, 2010, vol. 406, pp. 360–64.
26. W.L. Mankins, J.C. Hosier, and T.H. Bassford: *Metall. Trans.*, 1974, vol. 5, pp. 2579–90.
27. H.M. Tawancy: *J. Mater. Sci.*, 1992, vol. 27, pp. 6481–89.
28. Y.L. Lu, P.K. Liaw, G. Yang, M.L. Benson, S.A. Thompson, J.W. Blust, P.F. Browning, A.K. Bhattacharya, J.M. Aurrecoechea, and D.L. Klarstrom: *Mater. Sci. Eng. A*, 2005, vol. A397, pp. 122–31.
29. L.-Z. Ma and K.-M. Chang: *Scripta Mater.*, 2003, vol. 48, pp. 1271–76.
30. H.M. Tawancy: *Oxid. Met.*, 1996, vol. 45, nos. 3 and 4, pp. 323–48.
31. H. Ghonem and D. Zheng: *Mater. Sci. Eng. A*, 1992, vol. 150, pp. 151–60.
32. D.D. Krueger, S.D. Antolovich, and R.H. Van Stone: *Metall. Trans. A*, 1987, vol. 18A, pp. 1431–48.
33. L.A. Games: *Superalloy 718: Metallurgy and Applications*, Ed. E.A. Loria, TMS, Warrendale, PA, 1989, pp. 499–515.